PHYSICAL REVIEW D **80,** 023006 (2009)

Detection of exotic massive hadrons in ultrahigh energy cosmic ray telescopes

Ivone F. M. Albuquerque[1,2] and Washington R. Carvalho, Jr.[1]

[1]*Instituto de Física, Universidade de São Paulo, São Paulo, 05314, Brazil*

[2]*Center for Particle Astrophysics, Fermi National Accelerator Laboratory, Batavia, Illinois, 60510, USA*

(Received 30 January 2009; published 17 July 2009)

We investigate the detection of exotic massive strongly interacting hadrons (uhecrons) in ultrahigh energy cosmic ray telescopes. The conclusion is that experiments such as the Pierre Auger Observatory have the potential to detect these particles. It is shown that uhecron showers have clear distinctive features when compared to proton and nuclear showers. The simulation of uhecron air showers, and its detection and reconstruction by fluorescence telescopes, is described. We determine basic cuts in observables that will separate uhecrons from the cosmic ray bulk, assuming this is composed by protons. If these are composed by a heavier nucleus, the separation will be much improved. We also discuss photon induced showers. The complementarity between uhecron detection in accelerator experiments is discussed.

DOI: 10.1103/PhysRevD.80.023006 PACS numbers: 98.70.Sa, 14.80.−j, 13.85.−t, 96.50.sd

I. INTRODUCTION

Ultrahigh energy cosmic ray (UHECR) observatories investigate the high energy end of the cosmic ray spectrum (above $\sim 10^{19}$ eV). Their results [1,2] are consistent with the presence of the Greisen [3] and Zatsepin and Kuz'min [4] (GZK) feature.

GZK showed that nucleons propagating through the cosmic microwave background radiation will have their energy degraded. The main energy loss mechanism for cosmic rays above $\sim 5 \times 10^{19}$ eV is pion photoproduction. In order to reach the Earth, nucleons have to be produced relatively near us, at a maximum distance of about 100 Mpc. As a consequence, the cosmic ray energy spectrum should fall steeply around $\sim 5 \times 10^{19}$ eV. This feature is known as the GZK cutoff. As events above the expected cutoff were detected [5,6], the GZK cutoff was questioned. Telescopes optimized to search for higher energy events were built in order to understand if these events were or were not compatible with a flux suppression.

Here we investigate the possibility of detecting exotic massive and strongly interacting hadrons (uhecrons) in the Pierre Auger Observatory [7]. Uhecrons were first proposed [8] as a solution to the GZK [3,4] puzzle. Because of their greater mass, their threshold energy for pion photoproduction is larger than that for a proton. For this reason, an uhecron's energy degradation through the cosmic microwave background is much smaller when compared to a proton [8], and it can come from farther away. A thorough search [9] for the source of the highest energy cosmic ray ever detected (by the Fly Eye's Collaboration [10]) pointed to a faraway ($z = 0.545$) quasar (3C147) as one of the best candidates. Although a proton coming from this distance cannot reach the Earth, an uhecron can.

Uhecron candidates are found in extensions of the standard model of particle physics. Heavier uhecrons (masses >50 GeV) were excluded [11] as UHECR. Besides other reasons, the air showers they produce have their maximum too deep in the atmosphere. Among the surviving candidates are the heavy gluino lightest supersymmetric particle [12,13] and strongly interacting wimpless dark matter [14]. A search for the heavy gluino lightest supersymmetric particle using CDF [13] and LEP data [15] constrained its mass to a 25 to 35 GeV window. Here we show that the neutral mode of this particle can be detected by UHECR telescopes, and this mass window allows for discrimination from the bulk of UHECR assuming it is composed by protons or the nucleus.

Our investigation [16] follows the uhecron definition stated in [11]. It is an electrically neutral, strongly interacting heavy exotic hadron. The bulk of its mass is carried by a single constituent. This is surrounded by hadronic degrees of freedom, which are responsible for the uhecron interaction. This definition neither encompasses the archetypical uhecron S^0 [8,17,18], nor the gluino containing hadrons described in [19]. These particles have their momentum shared by their constituents in a different way than the uhecron.

We simulate uhecron induced air showers in a similar way as described in [11] and then simulate the detection and event reconstruction by a fluorescence detector (FD) as described in [20]. Proton and uhecron induced showers are compared, and their discriminating parameters are determined. As all UHECR simulations extrapolate known physics at lower energies to much larger energies, it is important to note that we compare uhecron to proton observables. In this way, we reduce the bias introduced due to uncertainties in the extrapolation of interaction models to high energies, since these uncertainties will affect both protons and uhecrons.

As a result, we show that uhecrons with masses below 50 GeV can be detected in UHECR telescopes and discriminated against protons and nucleus.

In the next section, we describe our simulation of uhecron induced showers. The description of the FD detection

and event reconstruction simulation follows. We then describe the main uhecron induced shower features and compare them to proton and iron induced showers. In Sec. IV, we describe how to discriminate between protons and uhecrons. In Sec. V we discuss photon induced showers. The last section presents our conclusions.

II. UHECRON INDUCED SHOWER SIMULATION

When a UHECR impinges Earth's atmosphere, it generates a shower of particles. As the shower develops, the number of particles increases until it reaches a maximum at a certain point in the atmosphere (Xmax). At this maximum, the energy of each particle is low enough to be lost through ionization. The development of the shower as a function of the atmospheric depth (longitudinal profile) depends on the primary cosmic ray composition. The longitudinal profile integrated energy is proportional to the primary cosmic ray energy.

Air shower simulations include a particle cascade development integrated with an event generator. The latter simulates the interactions between particles with the air nucleus while the shower development simulates the particle cascade versus atmospheric depth. In our simulation, we use the air shower extended simulations (AIRES) package (v2.8.4a) [21] with SIBYLL (v2.1) [22,23] as the event generator.

In order to simulate uhecron induced showers, we modified both AIRES and SIBYLL. While modifications to AIRES are straightforward, and basically require the inclusion of a new particle in the shower development, the modifications to the event generator are more complex. We use the modifications described in detail in [11].

SIBYLL [22] models the interaction of a particle with an air nucleus as a combination of a low energy hadron-hadron interaction and a model for the "hard" part of the cross section. It also models hadron-nucleus interactions [23]. The interactions that occur high in the atmosphere have very large center of mass energies. SIBYLL extrapolates the known physics at much lower energies to higher center of mass energies [$\vartheta(100\ \mathrm{TeV})$] using the dual parton model [24] superposed by the minijet production.

In short, the main modifications to SIBYLL (described in more detail in [11]) are as follows. The uhecron is represented as a heavy single constituent (Q) surrounded by light hadronic degrees of freedom. Its interaction is simulated in the same way as hadron-hadron interactions, which are represented [22] by production and fragmentation of QCD strings. However, uhecron interactions use harder structure and fragmentation functions than the ones used for normal hadrons. In analogy to the B meson, we describe the fraction of energy z carried by Q, using the Peterson fragmentation function [25,26]

$$f_Q(z) = \frac{1}{z}\left[1 - \frac{1}{z} - \frac{\varepsilon_Q}{1-z}\right]^{-2}, \tag{2.1}$$

where ε_Q is proportional to $\Lambda^2_{\mathrm{QCD}}/m^2_Q$.

The good agreement between this fragmentation function and data is described in [27]. This guarantees that most of the uhecron momentum is carried by the heavy constituent. The same function is used for the structure function, which describes the fraction of energy of the hadron carried by Q.

As the light constituents are responsible for the interactions, we take the uhecron-nucleon (σ_{UN}) cross section as the one for pion-nucleon interactions. Other modifications are related to diffraction dissociation, where the lower mass limit of the excited state was modified according to the uhecron mass (m_U). Also, the hard part of the cross section with large momentum transfer, which is

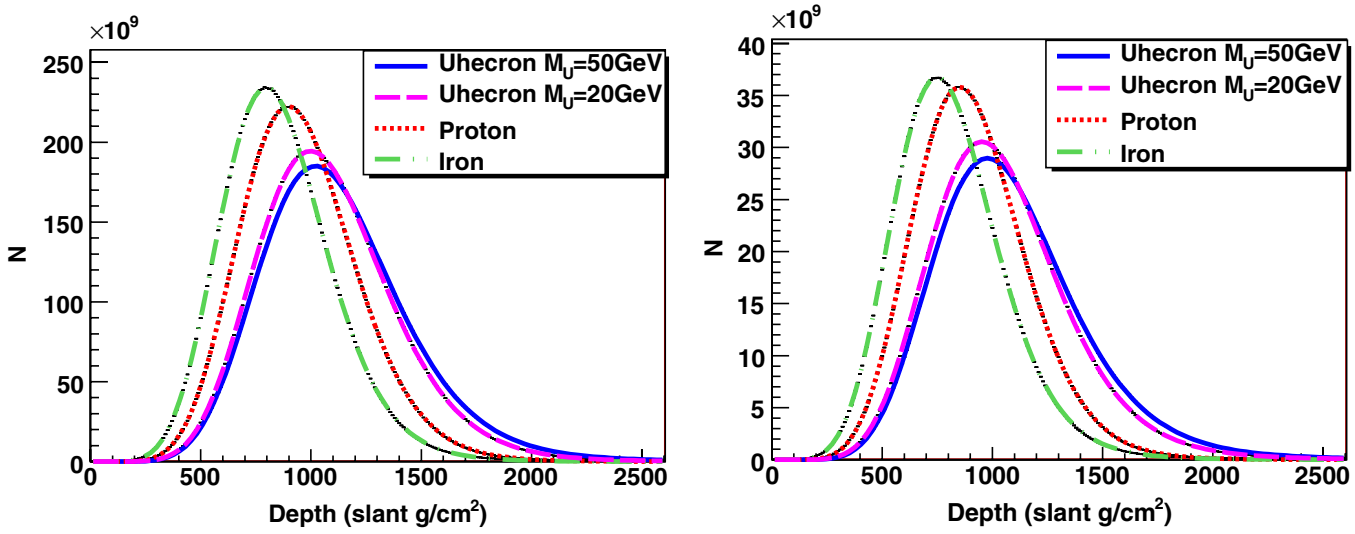

FIG. 1 (color online). Average longitudinal profiles based on 500 iron, proton, and uhecron (with $m_U = 20$ and 30 GeV) induced showers. Primary energies are equal to 320 (left) and 50 EeV (right). These showers were generated at a 60° zenith angle.

TABLE I. Nmax and Xmax (slant depth) for shower profiles shown in Fig. 1 and for a 30 GeV uhecron. Primary energies are 320 and 50 EeV.

Energy (EeV)	320		50	
Particle	Nmax ($\times 10^{11}$)	Xmax (g/cm^2)	Nmax ($\times 10^{10}$)	Xmax (g/cm^2)
Iron	2.34	797.1	3.68	749.4
Proton	2.23	897.6	3.58	852.1
Uhecron (20 GeV)	1.94	997.7	3.06	953.6
Uhecron (30 GeV)	1.92	1005.3	3.00	967.4
Uhecron (50 GeV)	1.85	1021.5	2.90	977.6

simulated as minijet production, is turned off for uhecrons, since most of the momentum is carried by Q which does not interact.

Figure 1 shows the average longitudinal profile of 320 and 50 EeV iron, proton, and uhecron (with $m_U = 20$ and 50 GeV) induced showers based on 500 showers for each primary. As uhecrons have less energy available for interactions than protons, its shower Xmax position is deeper in the atmosphere. As the uhecron mass increases, the available interaction energy decreases and the Xmax is deeper. These profiles show a fit with the Gaisser-Hillas [28] function (GH) to the simulated data.

The Xmax position and number of particles at this position (Nmax) of each average profile in Fig. 1 are shown in Table I. The average Xmax position of 20 GeV uhecrons is about 100 g/cm^2 deeper than the one for protons for both primary energies. Although the longitudinal profile fluctuates, it already indicates that uhecrons resemble more protons than the iron nucleus. For this reason we will determine ways to discriminate uhecrons from protons. Our distributions show that the same procedure will more efficiently separate them from iron.

Although the average longitudinal profile gives an idea of the general differences between proton and uhecron induced showers, the individual profile fluctuates a great deal. The Xmax distributions give a better idea of the fluctuation as well as the superposition among the different primaries. The Xmax distributions for proton and uhecron induced showers are shown in Fig. 2. As uhecrons interact always softly, the shower fluctuations are larger and the Xmax distribution is more spread out than for protons. This feature will help in the proton uhecron discrimination. However, as we will show in the next section, showers with an Xmax deeper than ground level are not accepted by the FD reconstruction. This requirement ends up lowering the uhecron acceptance.

III. SIMULATION OF FLUORESCENCE DETECTION AND EVENT RECONSTRUCTION

Fluorescence telescopes detect fluorescence photons emitted when charged particles transverse the atmosphere. As the air shower develops, the light emitted at different depths is collected by the FD photomultipliers (PMTs) and can be translated into an energy deposition longitudinal profile. The integration of this profile over the full shower path is proportional to the shower calorimetric energy. A small fraction ($\sim 10\%$) of the total shower energy is missed, since it is carried by neutrinos and by high energy muons which reach the ground.

After generating uhecron, proton, and iron induced showers, we simulate their detection by FDs. We use the

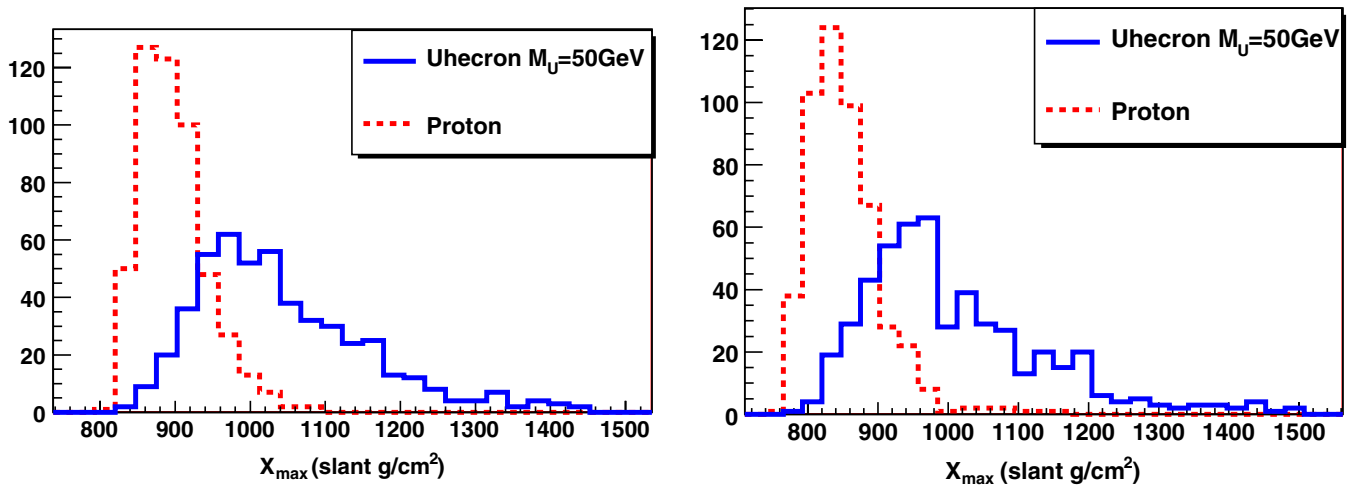

FIG. 2 (color online). Xmax distributions for 500 proton and 50 GeV uhecron induced showers of 320 (left) and 50 EeV (right).

TABLE II. Quality requirements over FD simulated data. Events that do not meet these requirements are cut. All but the GH χ^2 are found in [31]. Φ is the angle between the shower axis and the ground.

Quality Requirements	
Hit PMTs	>5
Track length	>200 g/cm^2
Zenith angle	$<60°$
Xmax	visible
Φ angle	$<132°$
χ^2 (GH fit)	<50

same FD simulation as described in [20], which followed the general procedure in [29]. As our simulation aims detection of rare events, a large coverage area is needed. For this reason we used the Pierre Auger FD parameters. The telescope altitude is set to 1500 m above sea level, 3.8 m^2 aperture covering an elevation angle from 2° to 32°, and using 1.5° pixel size PMTs. We take the telescope efficiency as 20%.

In short, our simulation [20] translates the shower energy deposited at each atmospheric depth into production of fluorescence photons. The propagation of these photons to the detector PMTs takes into account attenuation due to Rayleigh (molecular) and Mie (aerosol) scattering [30]. Details of fluorescence detection such as effective collection area, mirror reflectivity, filter transmission, phototube quantum efficiency, noise, and background are included. Once the sequence of signals in each PMT is determined, we simulate the energy reconstruction. We fold a 5° Gaussian error into the shower axis direction and transform back the PMT signal into deposited energy. All effects that were taken into account in the detection simulation are now determined by the new reconstruction shower geometry.

We generated 2000 showers for each primary at 3 energies (50, 100, and 320 EeV), all with a 60° zenith angle. Uhecrons with 20, 30, and 50 GeV mass were simulated. Each of these sets were used as inputs in the FD simulation. Each input was used 20 times, each with a different zenith angle and core position [20], in order to simulate an isotropic flux. Overall, 40K FD events were simulated for each energy and particle.

Once the longitudinal profile was reconstructed by the FD simulation a GH function was fit to determine the reconstructed energy. In order to cut badly reconstructed events, basic quality cuts were applied. These are listed in Table II and are always applied in our FD event reconstruction. All cuts except the GH fit χ^2 are typically used in Auger analysis [31]. The GH fit χ^2 was relaxed, since this fit is not as good for uhecron longitudinal profiles as for protons. Φ is the angle between the shower axis and the ground and is used to minimize the Cherenkov contamination.

Detection and energy reconstruction induces errors in the reconstructed longitudinal profile. Figure 3 compares the Xmax distributions for protons and 50 GeV uhecrons with 320 EeV primary energy, before and after the FD reconstruction. The distribution before the FD reconstruction fits a GH function directly to the data obtained by the air shower simulation (as described in Sec. II). This data is then reconstructed by the FD simulation as described in Sec. III. For a better visualization, we also show the distribution after FD reconstruction normalized to the number of input events.

The large reduction in the number of events comes from geometrical factors as well as from the quality requirements. The shower detection is largely dependent on the inclination of the shower, core position, and the detector field of view [20,32]. After the FD reconstruction, both proton and uhecron distributions are shifted to lower values and are also broader. The shift and reduction of events is weaker for protons when compared to uhecrons. While detection uncertainties broaden both proton and uhecron distributions, the FD acceptance favors lower Xmax values [32]. For this reason, more uhecron events are cut, and the

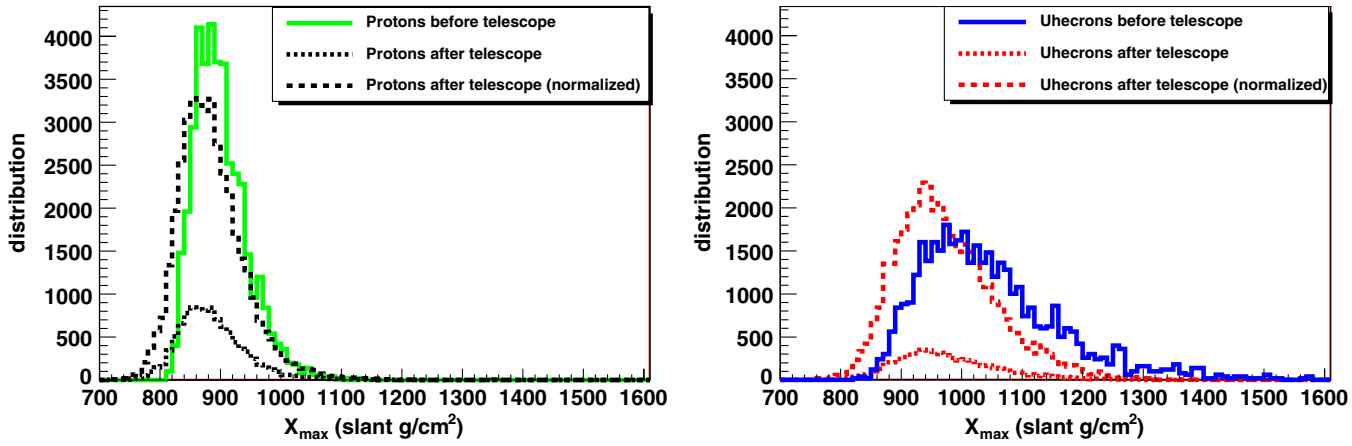

FIG. 3 (color online). Xmax distributions before and after FD reconstruction. Plots are for protons (left) and 50 GeV uhecrons (right) with 320 EeV primary energy.

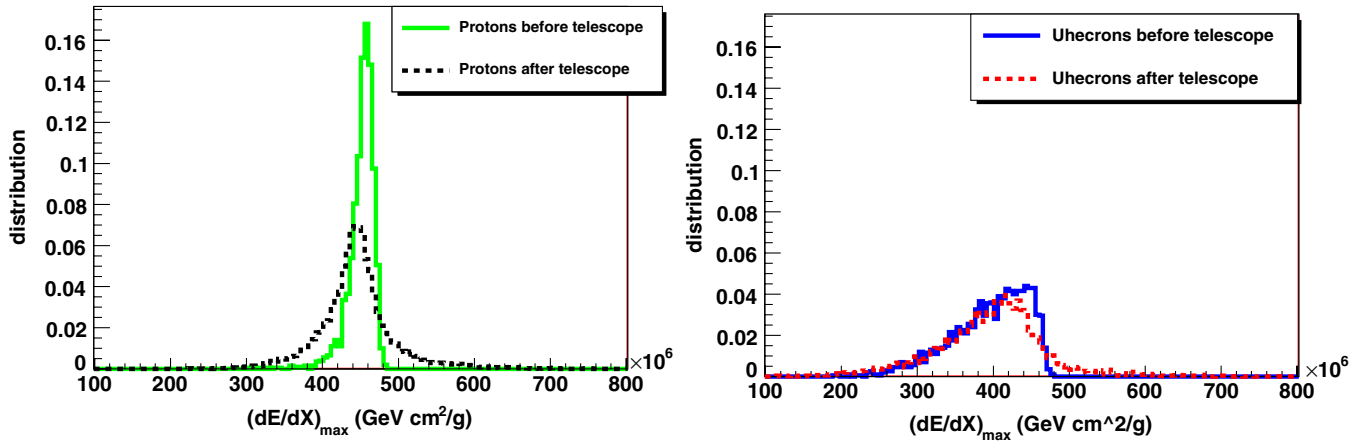

FIG. 4 (color online). Normalized maximum deposited energy distributions before and after FD reconstruction. Plots are for 320 EeV primary energy protons (left) and 50 GeV uhecrons (right). The dashed curves represent the distribution after the FD simulation normalized to the number of events before the FD simulation.

larger Xmax side of the distribution is less accepted. This shifts the distributions to lower Xmax values.

Since lower energy showers have an Xmax at higher altitudes, they will be less affected by the FD acceptance. Our distributions follow this trend: for lower primary energies, the Xmax distribution does not shift to lower values as much as for larger energies. Also, the reduction in the number of events is lower. While 84.7% (74.3%) of 320 EeV uhecrons (protons) are cut by the FD reconstruction, 81.5% (70.5%) of 100 EeV uhecrons (protons) are cut.

Figure 4 shows the normalized maximum deposited energy distributions (dE/dx) max before and after the FD reconstruction simulation for 320 EeV protons and uhecrons (with 50 GeV mass). As for the Xmax distributions, the maximum deposited energy also shifts to lower values. While the broadening of the proton distribution due to detection and reconstruction errors is clear on both sides, the effect on uhecrons is not that clear, especially at lower deposited energies. This can be explained by the inherent uhecron shower characteristics, which fluctuate much more than proton showers.

We also compare the reconstructed energy with the primary energy. The reconstructed energy is obtained by adding the missing energy to the calorimetric energy. While the latter is determined from the integration of the energy longitudinal profile, the missing energy is parametrized from Monte Carlo simulations. We used the same missing energy parametrization as determined for protons in [33]. Figure 5 shows the reconstructed energy error (given by $(E_{\mathrm{rec}}\text{-}E_{\mathrm{primary}})/E_{\mathrm{primary}}$) before and after the FD reconstruction. The energy error before the FD reconstruction includes the intrinsic errors in a basic energy reconstruction. It accounts for errors due to the GH fit, intrinsic shower fluctuations, and the missing energy parametriza-

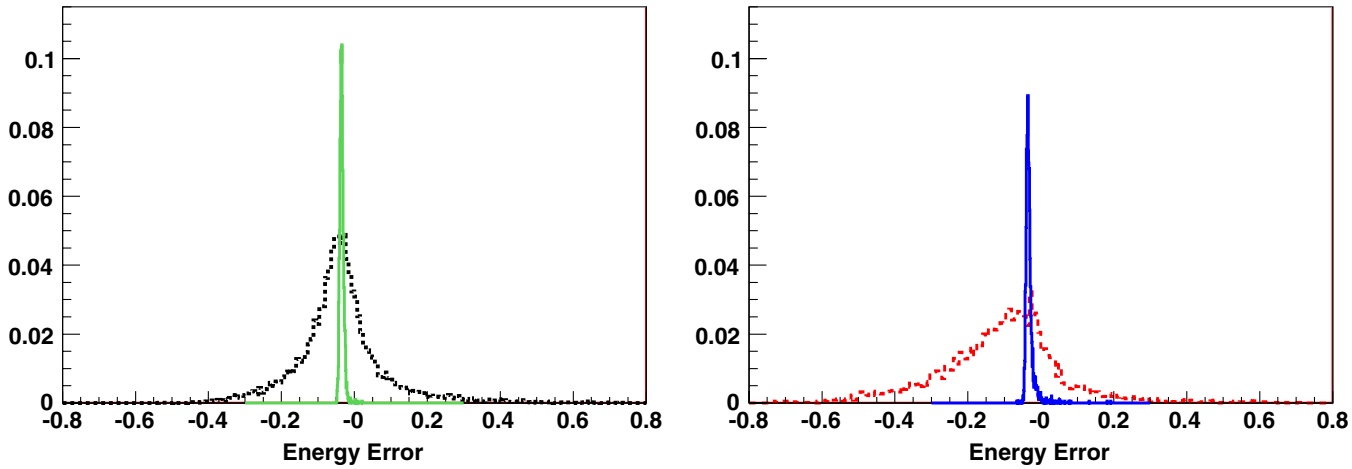

FIG. 5 (color online). Energy error distributions before and after FD reconstruction. Plots are for 320 EeV primary energy protons (left) and 50 GeV uhecrons (right). The green solid (proton) and solid narrow (uhecron) narrow distributions are the errors before FD reconstruction, while the dashed black (proton) and dashed red (uhecron) broad distributions are the errors after the FD reconstruction.

tion. An energy error of about 3% is already observed in the reconstructed energy before the FD simulation. This error is due to the missing energy parametrization, which was determined based on Corsika/QGSJET [34,35] simulations and generates this error when using AIRES/SIBYLL. Our investigation will not be biased by this error, since we always compare uhecrons with protons, and both are equally affected by the missing energy parametrization.

As also shown in Fig. 5, the proton energy error peaks at the same energy before and after the FD simulation. While it is symmetrically distributed, the uhecron distribution is asymmetric. The main reason for this is that the GH function is not the best fit for uhecron profiles. Among other problems, it does not account for the profile tail. In this analysis we did not attempt to find a better fit, but eventually it can help uhecron discrimination. As a result, uhecron showers will on average be reconstructed as lower energy showers, with a systematic energy error around -10%.

IV. UHECRON-PROTON DISCRIMINATION

As was shown in the previous section, the main characteristics of uhecron induced showers are a larger Xmax with less particles at this position (lower Nmax) and slower development when compared to proton induced showers. Here, we demonstrate the possibility of discriminating uhecron from proton induced showers using FD observables. Nucleus induced showers have an even smaller Xmax and are more easily discriminated from uhecrons.

Other than the Xmax and the (dE/dx) max (which has the same discriminating power as Nmax), the zenith angle θ_z and the altitude (Hmax), at which the first light is detected by the FD, can be used to discriminate uhecrons from protons.

It can be seen from Figs. 1 and 2 that uhecrons have deeper Xmax than protons. As a consequence, a large fraction of uhecron induced showers that come vertically into the atmosphere are cut by the FD reconstruction. The requirement that the shower Xmax is visible (see Table II) cuts most of the vertical uhecron showers. For this reason, uhecrons are better accepted at larger zenith angles, and a cut on low θ_z showers will be more effective on protons.

As described in Sec. II, most of the uhecron energy is not available for interactions. For this reason, its first interaction point with a deposited energy larger than the FD threshold will be deeper in the atmosphere than the first light collected from protons. Therefore Hmax can also be used as a discriminator.

Figures 6 and 7 show distributions for the observables used as uhecron discriminators. All distributions are after the FD reconstruction, for 320 EeV showers induced by protons and by 50 GeV uhecrons. These figures as well as Figs. 8 and 9 and Tables III and IV, are based on the same number of proton and uhecron induced showers that go into the FD simulation. We will discuss the effect of the ratio between the uhecron to proton flux in the next section.

In order to optimize all cuts on the discriminating parameters (which from here on we call analysis cuts), minimizing the background contamination, and maximizing the number of uhecrons, we use the following quality factor:

$$q = \frac{N_u}{(N_u + N_p)} \times N_u^a, \tag{4.1}$$

where N_u and N_p are the number of uhecrons and protons after all analysis cuts were applied, and a is a constant. Parameter a sets the strength of the cuts. It was set in an arbitrary way, requiring that a minimum amount of uhecrons were present in the final sample.

The quality factor q has to be maximized as a function of the analysis cuts. To achieve this maximization, we scan q over a fixed range for each of the discriminating parameters, Xmax, (dE/dx) max, Hmax, and θ_z. Each combination of cuts will yield a different q factor, and the

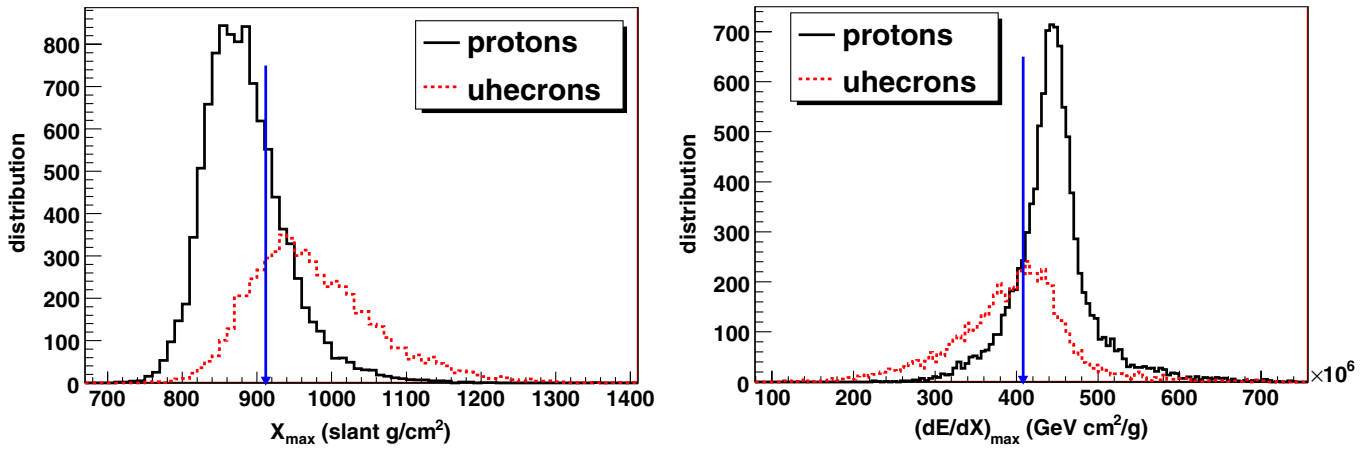

FIG. 6 (color online). Xmax (left) and (dE/dx) max (right) distributions after FD reconstruction for 320 EeV primary energy proton and 50 GeV uhecron induced showers. The arrows show the position of the optimized analysis cuts.

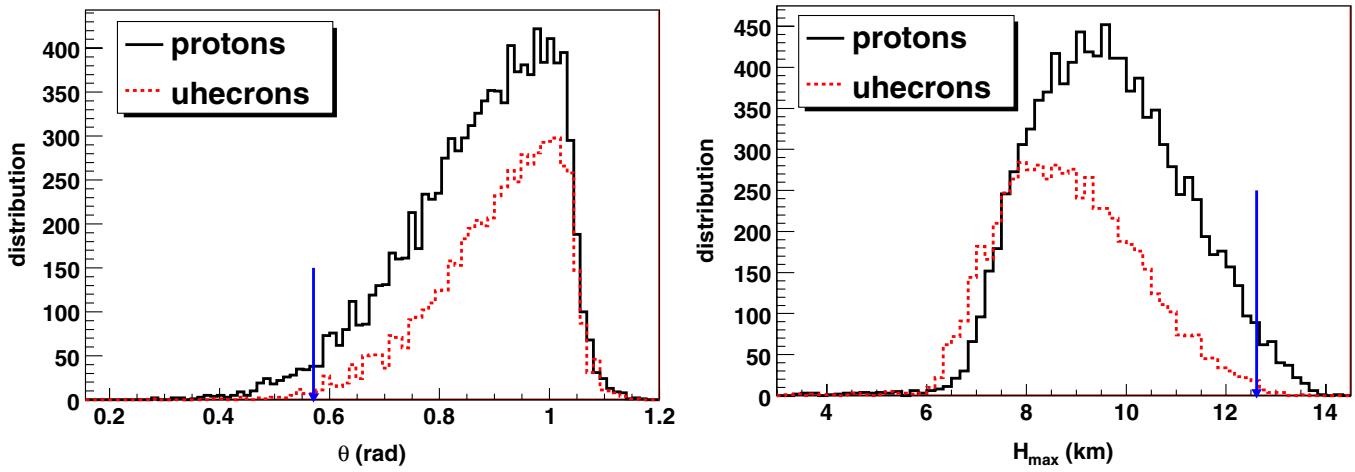

FIG. 7 (color online). θ_z (left) and Hmax (right) distributions after FD reconstruction for 320 EeV primary energy proton and 50 GeV uhecron induced showers. The arrows show the position of the optimized analysis cuts.

maximum value will indicate the optimized set of cuts. The arrows shown on Figs. 6 and 7 indicate the cut values on each of these parameters. Parameter a in Eq. (4.1) is set to 0.2.

Figure 8 shows the Xmax distribution for 320 EeV showers generated by protons and by 50 GeV uhecrons before and after the analysis cuts were applied. It shows the effectiveness of the analysis cuts, since most of the protons are cut while a significant uhecron fraction survives. The accepted region for each discriminating parameter, as well as the fraction of surviving events, are shown in Table III.

As discussed at the end of the previous section, uhecrons will have their primary energy reconstructed with about a 10% error to lower values. For this reason, we also compare 320 (100, 50) EeV proton showers with 352 (108, 54) EeV uhecron showers, corresponding to a 10% (8%) correction to the uhecron reconstructed energy. The results

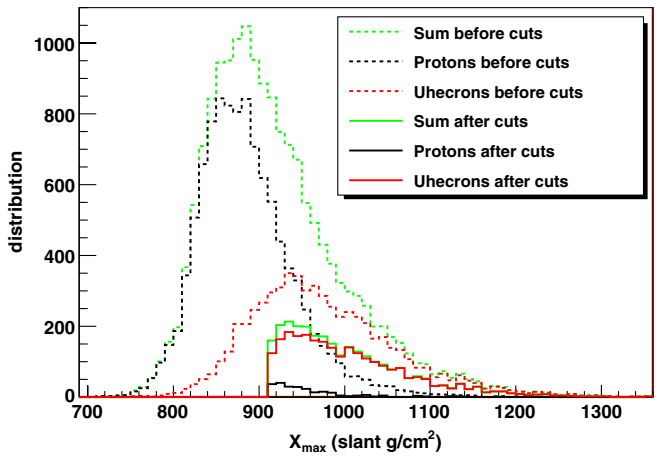

FIG. 8 (color online). Xmax distribution for protons and 50 GeV uhecrons of 320 EeV primary energy before and after analysis cuts were applied. Cut values and fraction of events surviving the cuts are shown in Table III.

are shown in Tables III and IV, where the first table compares 50 GeV and the latter 20 GeV uhecrons to protons.

Figure 9 shows both Xmax and (dE/dx) max distributions for 320 EeV protons and 50 GeV uhecrons with 320 and 352 EeV primary energy. The Xmax distribution will not change significantly, although it shifts slightly to deeper Xmax values. However, the (dE/dx) max distribution changes significantly, since the energy correction implies a larger deposited energy. This shift in the (dE/dx) max distribution will reduce the discriminating power of this observable.

Both uhecron energy and mass are important factors for discrimination from other primary particles. An energy increase favors deeper Xmax parameters, and therefore less FD acceptance, but on the other hand enhances the intrinsic differentiating shower characteristics in relation to protons. Lower uhecron masses approximate their shower intrinsic characteristics to proton showers, but increase the uhecron FD acceptance. As shown in Tables III and IV, it is possible to greatly reduce the proton contamination using Xmax, (dE/dx) max, Hmax, and θ_z as discriminating parameters. The proton contamination in the final event sample is at maximum 15% for 50 GeV uhecrons and below 20% for 20 GeV uhecrons.

A. Uhecron-proton flux ratio

Until now we have considered the same number of input uhecron and proton induced showers into the FD simulation. This is equivalent to an equal flux of protons and uhecrons arriving at the Earth. However, considering the latest UHECR flux measurements [1,2], a much lower uhecron flux has to be considered at least up to energies around the experimental value for the GZK cutoff. Beyond this point, a nucleon or nucleus flux is not expected. Events at energies beyond the GZK cutoff might indicate new physics.

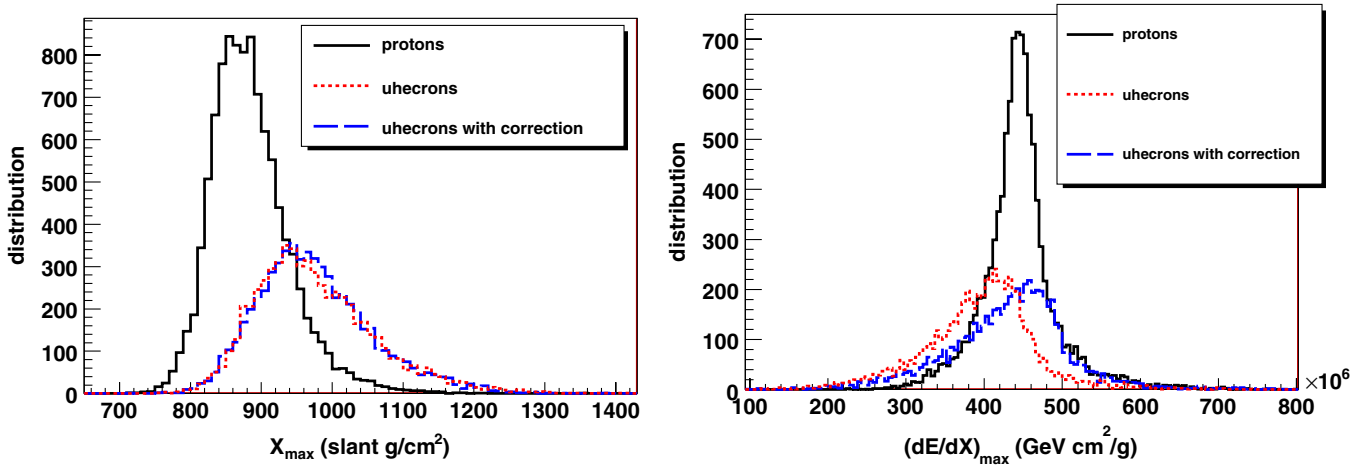

FIG. 9 (color online). Xmax (left) and (dE/dx) max (right) distributions after all analysis cuts were applied for 320 EeV protons and 50 GeV uhecrons with 320 and 352 EeV primary energy.

Here, we redo the analysis described in Sec. IV, but reducing the uhecron flux ϕ_u to 10%, 5%, and 1% relative to the proton flux ϕ_p. We analyze a 1% uhecron fraction for a 50 EeV primary energy (54 EeV for a uhecron shower), since at lower energies uhecrons might be present as a small fraction of the flux. Even in this scenario it is possible to discriminate uhecrons from protons. We summarize our results in Table V. In order to enhance the final number of uhecron events, we use larger a parameter values [see Eq. (4.1)]. After all analysis cuts are applied, the proton contamination in the final sample, for a 1% uhecron flux, is around 16%. As we will discuss in the last section, our results indicate the feasibility of discriminating uhecrons from protons, even with a much smaller uhecron flux.

B. Sample independence test

In order to check our uhecron analysis and the discriminating power of the Xmax, (dE/dx) max, θ max, and Hmax observables, we applied the same analysis cuts as described above to a new set of data. This new set of data uses the same 2000 showers generated from our shower simulation, for each primary particle (where 3 different uhecron masses—20, 30, and 50 GeV—were assumed) and for each different primary energy (50, 100, and 320 EeV), and inputs it with different geometry [20] than the original analysis to the FD simulation. The analysis cuts applied to this new simulated data set were the ones determined in the original analysis.

We obtain similar results as in the original analysis. The analysis cuts have the same discriminating power.

TABLE III. Fraction of events after analysis cuts. E_p and E_u are the primary energies (in EeV) of protons and 50 GeV uhecrons, respectively; $N_p(N_{p0})$, $N_u(N_{u0})$, and N_T are the number of protons; uhecrons and the sum of protons with uhecron induced showers after the FD simulation and after (before) all analysis cuts are applied. The last 4 columns indicate the accepted region for each discriminating parameter after cut optimization, in units of GeV cm^2/g, rad, km, and g/cm^2, respectively.

E_u	E_p	N_u/N_{u0}	N_p/N_{p0}	N_p/N_T	(dE/dx) max $>$	θ_Z $>$	Hmax $<$	Xmax $>$
320	320	0.417	0.022	0.081	4.08×10^8	0.571	12.61	912.2
352	320	0.402	0.043	0.152	5.20×10^8	0.633	11.50	973.3
108	100	0.366	0.039	0.143	157×10^8	0.637	11.44	956.3
54	50	0.299	0.016	0.080	6.64×10^7	0.400	11.41	882.8

TABLE IV. Same as in Table III but now uhecrons have 20 GeV mass.

E_u	E_p	N_u/N_{u0}	N_p/N_{p0}	N_p/N_T	(dE/dx) max $>$	θ_Z $>$	Hmax $<$	Xmax $>$
352	320	0.390	0.062	0.198	5.54×10^8	0.712	11.41	961.4
108	100	0.359	0.057	0.188	1.74×10^8	0.616	10.85	951.7
54	50	0.411	0.071	0.198	8.12×10^7	0.300	10.90	922.3

TABLE V. Fraction of events after analysis cuts for protons and 50 GeV uhecrons. ϕ_u/ϕ_p is the input ratio of uhecron to proton induced showers into the FD simulation. a is a parameter in Eq. (4.1), and all other parameters are described in Table III.

E_u	E_p	ϕ_u/ϕ_p	a	N_u/N_{u0}	N_p/N_{p0}	N_p/N_T
352	320	0.1	0.6	0.139	0.0023	0.219
352	320	0.05	0.5	0.102	0.0006	0.161
108	100	0.05	0.6	0.082	0.0006	0.184
108	100	0.05	0.7	0.162	0.0044	0.458
54	50	0.05	0.6	0.158	0.0015	0.234
54	50	0.01	0.8	0.081	0.0001	0.156

TABLE VI. Same as in Table III. Cuts are now applied to the new data set. Accepted region for each discriminating parameter was defined from the original data set. Uhecron mass was set to 50 GeV. Results with the original and with the new data set are compatible.

E_u	E_p	N_u/N_{u0}	N_p/N_{p0}	N_p/N_T	(dE/dx) max $>$	θ_Z $>$	Hmax $<$	Xmax $>$
352	320	0.395	0.044	0.164	5.20×10^8	0.633	11.50	973.3
320	320	0.414	0.025	0.090	4.08×10^8	0.571	12.61	912.2
108	100	0.358	0.042	0.156	1.57×10^8	0.637	11.44	956.3
54	50	0.306	0.019	0.090	6.64×10^7	0.400	11.41	882.8

TABLE VII. Same as in Table VI but now uhecrons have 20 GeV mass.

E_u	E_p	N_u/N_{u0}	N_p/N_{p0}	N_p/N_T	(dE/dx) max $>$	θ_Z $>$	Hmax $<$	Xmax $>$
352	320	0.390	0.062	0.198	5.54e + 08	0.712	11.41	961.4
108	100	0.359	0.057	0.188	1.74e + 08	0.616	10.85	951.7
54	50	0.411	0.071	0.198	8.12e + 07	0.300	10.90	922.3

Tables VI and VII summarize the analysis results for this new data set (for 50 and 20 GeV uhecrons, respectively). As can be seen, the results are compatible with the ones in Tables III and IV.

V. UHECRON-PHOTON COMPARISON

Photon showers develop deeper in the atmosphere than proton showers. For this reason it resembles more uhecron than proton induced showers. However, it is important to note that the competition among uhecrons and photons is not realistic. At these energies, both photons and uhecrons are proposed in beyond the standard model of particle physic scenarios. These either propose ultrahigh energy photons or exotic hadronic particles. It is already known that the photon fraction of the UHECR flux is very small, which constrain many top-down models [36]. In these models, ultrahigh energy photons would be produced from exotic heavy particle decay. Auger results limit [37] the photon fraction of the UHECR flux to 2% (5.1% and 31%) of the total flux above $1 \times (2 \times$ and $4\times)10^{19}$ eV with 95% confidence level.

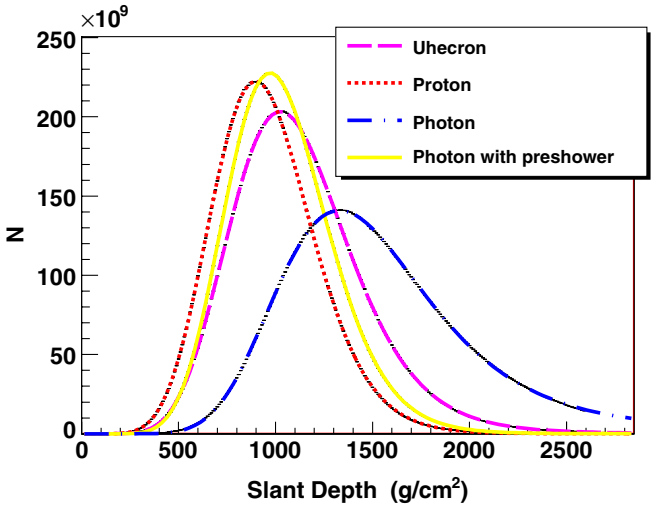

FIG. 10 (color online). Longitudinal profile for photon induced showers with and without the preshower effect. Proton and 50 GeV uhecrons are also shown. Proton and photon showers have 320 EeV primary energies, while uhecron has 352 EeV. All profiles are before FD reconstruction.

It is also important to note that photon induced showers develop differently from hadronic induced showers. This difference is mainly due to smaller particle multiplicity in the electromagnetic cascade when compared to a hadronic cascade. As a consequence, the photon shower Xmax is on average deeper than the proton Xmax. Also, the number of muons in hadronic showers is greater than in photon showers, due to charged pion decay. For this reason, an FD uhecron-photon discrimination can be greatly enhanced by ground detector information.

Another important effect to be taken into account is due to photon interactions with Earth's geomagnetic fields. As a consequence, they preshower before entering into the atmosphere. In Fig. 10 we compare proton, uhecron (with 50 GeV mass), and photon longitudinal profiles for 320 EeV induced showers. Photon profiles are shown with and without preshower. The effect seen in the longitudinal profile will be present in the Xmax distribution as well. The preshower effect changes both photon longitudinal and Xmax distributions in a way that it will resemble more uhecron showers than if this effect was not present. However, as mentioned above, the hadronic characteristics of uhecron showers might allow for their separation [38].

VI. DISCUSSION AND CONCLUSION

We have shown that UHECR experiments, such as those at the Pierre Auger Observatory, have the potential to detect exotic massive hadrons. We have also shown that it is possible to discriminate them from nucleon induced showers.

Although both proton and uhecrons produce hadronic showers, uhecron characteristics will allow discrimination from protons. As the uhecron mass increases, its induced shower develop more slowly and fluctuates more. The analysis of these characteristics allow to better distinguish heavier uhecron from proton showers, although it is also possible to distinguish lighter uhecrons. While the proton contamination in the final simulated data sample, after all analysis cuts are applied, is at maximum 15% for 50 GeV uhecrons, it is around 20% for 20 GeV uhecrons.

We have also shown the effects of fluorescence detection and event reconstruction. FD requirements can exclude uhecron showers that are naturally better discriminated from protons. However, even after FD detection and event reconstruction, it is possible to separate showers induced by these two primaries. We have shown that FD observables such as Xmax, (dE/dx) max, θ max, and Hmax, are good discriminators.

Although we have no prediction for the ratio between proton and uhecron induced showers, we have shown that the uhecron flux can be as small as 1% of the total flux and still be discriminated from protons. At lower primary energies, standard model particles should dominate the UHECR spectrum; whereas at energies beyond the GZK cutoff, it is possible to have a larger exotic flux.

It is important to note that the search for beyond standard model particles is complementary to accelerator searches. It depends on an assumed prior model. If the Large Hadron Collider (LHC) has indication of a heavy gluino [12,13], UHECR telescopes can look for it in a complementary way. Or vice versa, one can find uhecron candidates among UHECR and depending on LHC results, investigate its identity. Heavy gluino [12,13] and strongly interacting wimpless particles [14] are examples of uhecrons. The current allowed heavy gluino mass window [13] (25 to 35 GeV) is within the uhecron mass limits that allow separation from proton or nuclei background.

We have also shown that our method for uhecron detection and background reduction is independent from our simulated data. After our analysis method was determined, we applied it to a new data set. The new results show that our discriminating parameters have the same power as when they are applied to the original data set.

We have also compared uhecron to ultrahigh energy photon induced showers. Although it is not expected to have both of these particles as UHECR primaries, the differences between a hadronic and photon induced shower should allow for their discrimination [38]. Ground detectors should improve this discrimination.

As the uhecron flux at energies around the GZK cutoff has no reason to be large, the construction of the northern Auger site will definitely improve the uhecron detection probability.

ACKNOWLEDGMENTS

The authors thank Vitor de Souza for his useful comments. This work was partially funded by the State of São Paulo Research Foundation (FAPESP), the U.S. Department of Energy under Contracts No. DE-AC-76SF00098 and No. DE-AC02-07CH11359, and the Brazilian National Counsel for Scientific Research (CNPq).

[1] R. Abbasi *et al.*, Phys. Rev. Lett. **100**, 101101 (2008).
[2] T. Yamamoto (Pierre Auger Collaboration), arXiv:0707.2638.
[3] K. Greisen, Phys. Rev. Lett. **16**, 748 (1966).
[4] G. T. Zatsepin and V. A. Kuz'min, JETP Lett. **4**, 78 (1966) [Pis'ma Zh. Eksp. Teor. Fiz **4**, 114 (1966)].
[5] M. Takeda *et al.*, Phys. Rev. Lett. **81**, 1163 (1998).
[6] R. U. Abbasi *et al.*, Astropart. Phys. **23**, 157 (2005).
[7] V. V. Elewyck, Mod. Phys. Lett. A **23**, 221 (2008).
[8] D. J. H. Chung, G. F. Farrar, and E. W. Kolb, Phys. Rev. D **57**, 4606 (1998).
[9] J. W. Elbert and P. Sommers, Astrophys. J. **441**, 151 (1995).
[10] D. J. Bird *et al.* (HIRES Collaboration), Astrophys. J. **424**, 491 (1994).
[11] I. F. M. Albuquerque, G. R. Farrar, and E. W. Kolb, Phys. Rev. D **59**, 015021 (1998).
[12] S. Raby, Phys. Lett. B **422**, 158 (1998).
[13] A. Mafi and S. Raby, Phys. Rev. D **62**, 035003 (2000).
[14] J. L. Feng and J. Kumar, Phys. Rev. Lett. **101**, 231301 (2008).
[15] H. Baer, K. m. Cheung, and J. F. Gunion, Phys. Rev. D **59**, 075002 (1999).
[16] W. J. Carvalho, Ph.D. thesis, University of São Paulo, 2008 (in Portuguese), http://www.teses.usp.br/teses/disponiveis/43/43134/tde-13102008-102648/.
[17] G. R. Farrar, Phys. Rev. Lett. **76**, 4111 (1996).
[18] Although the light gluino scenario has been excluded by three experiments (E761, ALEPH, and KTeV), we find it important to clarify its distinction to the uhecron picture we assume in this paper.
[19] V. Berezinsky and M. Kachelriess, Phys. Lett. B **422**, 163 (1998); V. Berezinsky, M. Kachelriess, and S. Ostapchenko, Phys. Rev. D **65**, 083004 (2002).
[20] W. J. Carvalho, I. F. M. Albuquerque, and V. de Souza, Astropart. Phys. **28**, 89 (2007).
[21] S. J. Sciutto, arXiv:9911331.
[22] R. S. Fletcher, T. K. Gaisser, P. Lipari, and T. Stanev, Phys. Rev. D **50**, 5710 (1994); R. Engel, T. K. Gaisser, T. Stanev, and P. Lipari, in *Proceedings of the 26th International*

Cosmic Ray Conference (AIP Conference Proceedings, Salt Lake City, Utah, 1999), Vol. 1, p. 415.
[23] J. Engel, T. K. Gaisser, T. Stanev, and P. Lipari, Phys. Rev. D **46**, 5013 (1992).
[24] A. Capella and A. Krzywicki, Phys. Rev. D **18**, 3357 (1978).
[25] C. Peterson, D. Schlatter, I. Schmitt, and P. M. Zerwas, Phys. Rev. D **27**, 105 (1983).
[26] W. M. Yao *et al.* (Particle Data Group), J. Phys. G **33**, 1 (2006).
[27] D. Buskulic *et al.* (ALEPH Collaboration), Phys. Lett. B **357**, 699 (1995).
[28] T. K. Gaisser and A. M. Hillas, in *Proceedings of the 15th International Cosmic Ray Conference* (Bulg. Acad. Sci., Plovdiv, Bulgaria, 1977), Vol. 8, p. 353.
[29] V. de Souza, G. Medina-Tanco, and J. A. Ortiz, Phys. Rev. D **72**, 103009 (2005).
[30] F. Kakimoto, E. C. Loh, M. Nagano, H. Okuno, M. Teshima, and S. Ueno, Nucl. Instrum. Methods Phys. Res., Sect. A **372**, 527 (1996).
[31] P. Sommers (Pierre Auger Collaboration), arXiv:astro-ph/0507150.
[32] A. S. Chou, Phys. Rev. D **74**, 103001 (2006).
[33] H. M. J. Barbosa, F. Catalani, J. A. Chinellato, and C. Dobrigkeit, Astropart. Phys. **22**, 159 (2004).
[34] D. Heck, G. Schatz, T. Thouw, J. Knapp, and J. N. Capdevielle, Forschungszentrum Karlsruhe Report No. FZKA6019, 1998, http://www-ik.fzk.de.
[35] N. N. Kalmykov, S. S. Ostapchenko, and A. I. Pavlov, Nucl. Phys. B, Proc. Suppl. **52**, 17 (1997).
[36] P. Bhattacharjee and G. Sigl, Phys. Rep. **327**, 109 (2000).
[37] J. Abraham *et al.* (Pierre Auger Collaboration), Astropart. Phys. **29**, 243 (2008).
[38] I. F. M. Albuquerque, W. J. Carvalho, and V. de Souza (unpublished).